Check for updates

Concerted suppressive effects of carisbamate, an anti-epileptic alkyl-carbamate drug, on voltage-gated Na$^+$ and hyperpolarization-activated cation currents

Te-Yu Hung[1], Sheng-Nan Wu[2,3,4]* and Chin-Wei Huang[5]*

[1]Department of Pediatrics, Chi Mei Medical Center, Tainan, Taiwan, [2]Department of Physiology, College of Medicine, National Cheng Kung University, Tainan, Taiwan, [3]College of Medicine, Institute of Basic Medical Sciences, National Cheng Kung University, Tainan, Taiwan, [4]School of Medicine, College of Medicine, National Sun Yat-sen University, Kaohsiung City, Taiwan, [5]Department of Neurology, National Cheng Kung University Hospital, College of Medicine, National Cheng Kung University, Tainan, Taiwan

Carisbamate (CRS, RWJ-333369) is a new anti-seizure medication. It remains unclear whether and how CRS can perturb the magnitude and/or gating kinetics of membrane ionic currents, despite a few reports demonstrating its ability to suppress voltage-gated Na$^+$ currents. In this study, we observed a set of whole-cell current recordings and found that CRS effectively suppressed the voltage-gated Na$^+$ (I_{Na}) and hyperpolarization-activated cation currents (I_h) intrinsically in electrically excitable cells (GH$_3$ cells). The effective IC$_{50}$ values of CRS for the differential suppression of transient ($I_{Na(T)}$) and late I_{Na} ($I_{Na(L)}$) were 56.4 and 11.4 μM, respectively. However, CRS strongly decreased the strength (i.e., Δarea) of the nonlinear window component of I_{Na} ($I_{Na(W)}$), which was activated by a short ascending ramp voltage (V_{ramp}); the subsequent addition of deltamethrin (DLT, 10 μM) counteracted the ability of CRS (100 μM, continuous exposure) to suppress $I_{Na(W)}$. CRS strikingly decreased the decay time constant of $I_{Na(T)}$ evoked during pulse train stimulation; however, the addition of telmisartan (10 μM) effectively attenuated the CRS (30 μM, continuous exposure)-mediated decrease in the decay time constant of the current. During continued exposure to deltamethrin (10 μM), known to be a pyrethroid insecticide, the addition of CRS resulted in differential suppression of the amplitudes of $I_{Na(T)}$ and $I_{Na(L)}$. The amplitude of I_h activated by a 2-s membrane hyperpolarization was diminished by CRS in a concentration-dependent manner, with an IC$_{50}$ value of 38 μM. For I_h, CRS altered the steady-state $I-V$ relationship and attenuated the strength of voltage-dependent hysteresis (Hys$_{(V)}$) activated by an inverted isosceles-triangular V_{ramp}. Moreover, the addition of oxaliplatin effectively reversed the CRS-mediated suppression of Hys$_{(V)}$. The predicted docking interaction between CRS and with a model of the hyperpolarization-activated cyclic nucleotide-gated (HCN) channel or between CRS and the hNa$_V$1.7 channel reflects the ability of CRS to bind to amino acid residues in HCN or hNa$_V$1.7 channel via hydrogen bonds and

hydrophobic interactions. These findings reveal the propensity of CRS to modify $I_{Na(T)}$ and $I_{Na(L)}$ differentially and to effectively suppress the magnitude of I_h. I_{Na} and I_h are thus potential targets of the actions of CRS in terms of modulating cellular excitability.

1. Introduction

Carisbamate (CRS, RWJ-333369), a bioactive, orally administered neuromodulator, has been demonstrated to be beneficial for the treatment of different types of convulsive disorders, including drug-resistant focal epilepsy and partial-onset seizure (Whalley et al., 2009; Sperling et al., 2010; Vohora et al., 2010; Ono et al., 2011; Faure et al., 2013, 2014; Fernandes et al., 2015; Marques-Carneiro et al., 2017; Steriade et al., 2020; Löscher et al., 2021; Lu et al., 2021; Strzelczyk and Schubert-Bast, 2021; Elkommos and Mula, 2022; Pong et al., 2022). This compound was also reported to be effective in the treatment of alcoholism (Rezvani et al., 2009, 2012). One study found that CRS prevented the development and production of epilepsy-like discharges and exerted a neuroprotective effect after epilepticus-like injury (Fernandes et al., 2015).

CRS was demonstrated to suppress glutamate transmission in granule cells of the dentate gyrus (Lee et al., 2011). It also was reported to effectively suppress action potential firing and exert neuroprotective effects in either cultured hippocampal neurons or a rat model of status epilepticus (Deshpande et al., 2008a,b, 2016a,b; Fernandes et al., 2015; Deshpande and DeLorenzo, 2020). Alternatively, CRS can inhibit voltage-gated Na$^+$ channels (Liu Y. et al., 2009; Whalley et al., 2009; Vohora et al., 2010; Shim et al., 2013). One paper reported the ability of CRS to suppress T-type voltage-gated Ca^{2+} currents (Kim et al., 2017). Hence, it remains unclear whether and how CRS can perturb ionic currents.

The magnitude of the voltage-gated Na$^+$ current (I_{Na}) through voltage-gated Na$^+$ (Na$_V$) channels is crucial to the generation and propagation of action potentials in excitable membranes (Catterall et al., 2020; Menezes et al., 2020). During abrupt depolarization, these channels become activated and can shift quickly from a resting (or closed) to an open state, thereby allowing the flow of Na$^+$ ions from the extracellular solution to the cell interior under electrochemical driving forces. Na$^+$ channels that have been opened in a voltage-dependent manner then shift to an inactive state, resulting in the transient enhancement of I_{Na}. In addition to the voltage dependence of slow I_{Na} inactivation, studies have reported the striking cumulative inhibition of the current activated during pulse train stimulation (Taddese and Bean, 2002; Huang et al., 2015; Navarro et al., 2020; Lin et al., 2022; Wu et al., 2022a). At present, it remains unclear whether and how CRS can interact with Na$_V$ channels to modify the magnitude, gating kinetics, and frequency-dependence of I_{Na}.

The hyperpolarization-activated cation current, I_h (i.e., the funny current [I_f]), is a key determinant of repetitive electrical activity in heart cells and various types of central neurons and endocrine or neuroendocrine cells (Belardinelli et al., 1988; Irisawa et al., 1993; Simasko and Sankaranarayanan, 1997; Stojilkovic et al., 2010; Kretschmannova et al., 2012; Wu and Huang, 2021; Choi et al., 2022; Chuang et al., 2022; Depuydt et al., 2022; Peters et al., 2022). This ionic current has unusually slow voltage-dependent activation kinetics and is a mixed, inwardly directed Na$^+$/K$^+$ current that is sensitive to blocking by CsCl or ivabradine (Cao et al., 2016; Hsiao et al., 2019). Activation of I_h may cause the resting potential to depolarize and, in turn, reach the threshold required to generate or elicit an action potential; as a result, I_h can affect pacemaker activity and impulse propagation (Anastasaki et al., 2022; Lei et al., 2022; Peters et al., 2022). Moreover, the slow kinetics of I_h in response to a long hyperpolarizing step can produce long-lasting, activity-dependent modification of membrane excitability in different excitable cell types (Kretschmannova et al., 2012; Peters et al., 2021; Mäki-Marttunen and Mäki-Marttunen, 2022). I_h is transmitted through channels encoded by members of the hyperpolarization-activated cyclic nucleotide-gated (HCN) gene family, and studies have shown that the activity of these channels is responsible for the ionic mechanisms of different convulsive disorders (Noam et al., 2011; Banarroch, 2013; Concepcion et al., 2021).

In this study, we extensively investigated the electrophysiological actions of CRS in excitable cells with consideration of the above-described information. We aimed to investigate the intrinsic effects of CRS on the magnitude and/or gating of I_{Na} or I_h in GH$_3$ neuronal cells. Our findings prompt us to consider both I_{Na} and I_h in excitable cells as distinctive targets of CRS, through which it can act concertedly to influence the functional activities of the cells involved.

2. Materials and methods

2.1. Chemicals, drugs, reagents, and solutions used in this work

Carisbamate (CRS; also known as Comfyde^{TM}, RWJ-333369, YKP 509, [(2S)-2-(2-chlorophenyl)-2-hydroxyethyl] carbamate, (S)-2-O-carbamoyl-1-o-chlorophenyl-ethanol, C$_9$H$_{10}$ClNO$_3$) and deltamethrin (DLT) were acquired from MedChemExpress (MCE$^®$; Everything Biotech, New Taipei City, Taiwan). Telmisartan (Tel) was obtained from Tocris Cookson Ltd. (Bristol, UK). Oxaliplatin (OXAL) was obtained from Sanofi-Aventis (New York,

NY, USA). Nimodipine, tetraethylammonium chloride (TEA), and tetrodotoxin (TTX) were obtained from Sigma-Aldrich (St. Louis, MO, USA). Chlorotoxin was a gift from Prof. Dr. Woei-Jer Chuang (Department of Biochemistry, National Cheng Kung University Medical College, Tainan, Taiwan). Other chemicals (e.g., CsCl, CsOH, and CdCl$_2$) and reagents used in this work were obtained from commercial sources and of reagent grade. Reagent-grade water was de-ionized using a Milli-Q$^®$ water purification system (Millipore, Bedford, MA, USA).

HEPES-buffered normal Tyrode's solution was used as the electrophysiological bath solution, with an ionic composition of (in mM): NaCl, 136.5; KCl, 5.4; MgCl$_2$, 0.53; CaCl$_2$, 1.8; glucose, 5.5; and HEPES-NaOH buffer, 5.5 (pH 7.4). The intracellular pipette solution used to measure the ions flowing through the whole-cell K$^+$ current or hyperpolarization-activated inward current (I_h) had the following composition (in mM): Potassium aspartate, 130; KCl, 20; MgCl$_2$, 1; Na$_2$ATP, 3; Na$_2$GTP, 0.1; EGTA, 0.1; and HEPES-KOH buffer, 5 (pH 7.2). To record different types of voltage-gated Na$^+$ current (I_{Na}), we replaced K$^+$ ions in the internal solution with equimolar Cs$^+$ ions and titrated the pH value to 7.2 by adding CsOH; the studied cells were commonly bathed in Ca^{2+}-free Tyrode's solution containing 10 mM TEA. Generally, the bath and pipette solutions were filtered on the day of use through a syringe filter equipped with a 0.22-μm Supor$^®$ nylon membrane (#4612; Pall Corp.; Genechain, Kaohsiung, Taiwan).

2.2. Cell preparation

The GH$_3$ pituitary cell line (BCRC-60015) was obtained from the Bioresources Collection and Research Center (Hsinchu, Taiwan). The cells were maintained in 50-mL plastic culture flasks in Ham's F-12 medium supplemented with 2.5% fetal calf serum (*v/v*), 15% horse serum (*v/v*), and 2 mM glutamine (Wu et al., 2017; Hung et al., 2021). The medium was replaced twice weekly, and the cells were carefully split into subcultures once weekly. The cells were subjected to electrophysiological measurements when they reached 60%–80% confluence (5 or 6 days after subculture).

2.3. Electrophysiological measurements (patch-clamp recordings)

Shortly before each measurement, the GH$_3$ cells were carefully dispersed. A few drops of the cell suspension were rapidly transferred to a custom-built chamber, and the cells were allowed to settle on the bottom surface. The chamber used to record was tightly mounted on the stage of an inverted phase-contrast microscope (Diaphot-200; Nikon; Lin Trading Co., Taipei, Taiwan) coupled to a video camera system (magnification: 1500×) to monitor cell size during the experiments. The cells were kept at room temperature (20–25°C) in a bath of normal Tyrode's solution containing 1.8 mM CaCl$_2$. The patch electrodes were carefully drawn from Kimax-51 capillaries with an outer diameter of 1.5–1.8 mm (#34500; Kimble; Dogger, New Taipei City, Taiwan) using a two-stage PP-83 puller (Narishige; Taiwan Instrument, Tainan, Taiwan), and the electrode tips were fire-polished with an MF-83 microforge (Narishige). Once filled with different pipette solutions

as described in the section "2.1. Chemicals, drugs, reagents, and solutions used in this work," the tip resistance of the electrodes generally ranged from 3 to 5 MΩ. We used an RK-400 patch amplifier (Bio-Logic, Claix, France) to perform standard patch-clamp recordings in a modified whole-cell configuration (Lai et al., 2020, 2022). Junction potentials, which develop at the electrode tip when the composition of the internal solution differs from that in the bath, were nullified shortly before seal formation was made, and junction potential corrections were applied to the whole-cell data. While recording, the signal output data (i.e., potential or current tracings) were stored online at a frequency of $\geq$10 kHz using an ASUSPRO-BN401 LG laptop computer (ASUS; Yun-Dai, Tainan, Taiwan) equipped with a Digidata 1440A device (Molecular Devices; Advanced Biotech, New Taipei City, Taiwan) and controlled by pCLAMP 10.6 software (Molecular Devices).

2.4. Data analyses

We constructed and then analyzed the concentration–response curves of CRS-mediated inhibition on the peak (transient, $I_{Na(T)}$) and sustained (late, $I_{Na(L)}$) components of depolarization-activated I_{Na} and the hyperpolarization-activated inward current (I_h) present in GH$_3$ cells. The I_{Na} was evoked by a 30-ms depolarizing pulse to −10 mV from a holding potential of −100 mV, and the current amplitudes were measured at the start ($I_{Na(T)}$) and end ($I_{Na(L)}$) of the depolarizing pulse in the presence or absence of exposure to different CRS concentrations. The I_h was activated slowly by a 2-s hyperpolarizing step from −40 to −110 mV, and the current amplitude was measured at the end of the hyperpolarizing command voltage. The concentration of CRS needed to inhibit 50% of the current amplitude (IC$_{50}$) was approximated using the three-parameter logistic model, a modified form of the sigmoidal Hill equation, with goodness-of-fitness assessments as follows:

Relative amplitude =

$$\left\{[CRS]^{-n_H} \times (1-a)\right\}/\left\{[CRS]^{-n_H} + IC_{50}^{-n_H}\right\} + a$$

In this equation, [*CRS*] = the CRS concentration, n_H = the Hill coefficient, and 1 – *a* represents the maximal inhibition.

2.5. Curve-fitting procedures and statistical analyses

Linear or nonlinear (e.g., exponential of sigmoidal function) regression was used to fit continuous curves to the experimental data, using pCLAMP 7 software (Molecular Devices), 64-bit OriginPro 2022b software (OriginLab$^®$; Scientific Formosa, Kaohsiung, Taiwan), or Excel 2016 software (Microsoft, Redmond, WA, USA) with the "Solver" add-in function. The experimental data consist of different types of ionic currents and are presented as the mean ± standard error of the mean (SEM). The sample size (n) indicates the number of cells from which data were collected; and SEM error bars were plotted. The Kolmogorov Smirnov test for normality indicated that the data distribution obtained was satisfactory. To assess differences between more than two groups, we used an analysis of variance (ANOVA-1 or ANOVA-2) with

or without repeated measures, followed by a *post-hoc* Fisher's least significant difference test. Differences were considered statistically significant at a *p*-value < 0.05.

2.6. Docking studies

To explore the docking prediction, we first selected the structure from PDB (PDB: 5V4S) and entered it into the PyRx software. We also selected the chemical structure from PubChem (Compound CID: 6918474) and entered it into PyRx. After that, we performed appropriate docking actions in PyRx. Subsequently, we selected the results of this interaction and used LigPLOT+ software to generate an image that predicted the docking.

3. Results

3.1. Suppressive effect of carisbamate on the voltage-gated Na+ current (I_{Na})

In our initial whole-cell experiments, we examined whether CRS exerted any effects on I_{Na} in pituitary GH$_3$ cells. To avoid contamination by Ca^{2+} currents, the cells were bathed in Ca^{2+}-free Tyrode's solution containing 10 mM TEA and 0.5 mM CdCl$_2$, and the recording electrode was filled with a Cs$^+$-containing internal solution. In the recording pipette, Cl$^-$ ions were replaced with aspartate to eliminate any possible contamination by Cl$^-$ currents, because CRS was reported to alter the magnitude of Cl$^-$ currents (Whalley et al., 2009). As demonstrated in **Figure 1A**, after exposure of GH$_3$ cells to CRS for 1 min at a concentration of 10 or 30 µM, the amplitudes of $I_{Na(T)}$ and $I_{Na(L)}$ decreased from the control values of 813 ± 15 pA (*n* = 7) and 9.7 ± 0.3 pA (*n* = 7), respectively, to 598 ± 11 pA (*n* = 7, *p* < 0.05) and 4.4 ± 0.2 pA (*n* = 7, *p* < 0.05), and to 485 ± 9 pA (*n* = 7, *p* < 0.05) and 2.5 ± 0.1 pA (*n* = 7, *p* < 0.05), respectively. After the removal of CRS, the amplitudes of $I_{Na(T)}$ and $I_{Na(L)}$ returned to 801 ± 14 (*n* = 7, *p* < 0.05) and 9.5 ± 0.2 pA (*n* = 7, *p* < 0.05), respectively. Continuous exposure of the cells to 1 µM TTX alone, but not to 1 µM nimodipine alone, nearly eliminated the $I_{Na(T)}$ amplitude in response to the same voltage protocol, as demonstrated by a reduction from the control value of 814 ± 16 pA to 31 ± 5 pA (*n* = 7, *p* < 0.01). Concomitant with changes in the amplitude of $I_{Na(T)}$ or $I_{Na(L)}$, CRS (30 µM) decreased the time constant for the slow component of $I_{Na(T)}$ inactivation ($\tau_{inact(S)}$) from 9.5 ± 0.4 to 4.2 ± 0.4 ms (*n* = 7, *p* < 0.05); however, no clear change in the time constant for the fast component of current inactivation was observed.

Figure 1B demonstrates that exposure to CRS can decrease the amplitudes of $I_{Na(T)}$ and $I_{Na(L)}$ evoked by a rapid depolarizing pulse in a concentration-dependent manner. According to the modified Hill equation detailed in the section "2.4. Data analyses," the IC$_{50}$ value needed for CRS-mediated suppression of $I_{Na(T)}$ or $I_{Na(L)}$ from GH$_3$ cells was calculated as 56.4 or 11.4 µM, respectively, and these distinct values demonstrate the difference between the inhibitory effects of CRS on the magnitudes of $I_{Na(T)}$ and $I_{Na(L)}$ in these cells. Therefore, as observed during

a rectangular depolarizing step, this drug exhibits a preferential inhibition of $I_{Na(L)}$ over $I_{Na(T)}$ when activated.

3.2. Effect of CRS on the steady-state current versus voltage ($I–V$) relationship of $I_{Na(T)}$

To further characterize the inhibitory effect of CRS, we explored whether this drug could alter the steady-state $I–V$ relationship of $I_{Na(T)}$ in GH$_3$ cells. **Figure 2** illustrates the average $I–V$ relationship of $I_{Na(T)}$ in the presence or absence of 30 µM CRS. Notably, the value of the threshold or maximal voltage required to elicit $I_{Na(T)}$ did not differ between the absence and presence of CRS. Accordingly, we conclude that continuous exposure to CRS does not elicit an obvious change in the quasi-steady-state $I–V$ relationship of $I_{Na(T)}$, despite a significant reduction in $I_{Na(T)}$ conductance.

3.3. Suppressive effect of CRS on the window component of I_{Na} ($I_{Na(W)}$)

Instantaneous $I_{Na(W)}$, which is activated in response to an upsloping (or ascending) ramp voltage (V_{ramp}), has been demonstrated in different types of excitable cells (Morris et al., 2012; Yu et al., 2012; Wu et al., 2022a). We next examined whether CRS could alter the magnitude of $I_{Na(W)}$ evoked by a rapidly ascending V_{ramp}. In this set of experiments, we voltage-clamped the studied cell at −80 mV and applied an ascending V_{ramp} from −100 to +40 mV for a duration of 50 ms (ramp speed = 2.8 mV/ms) to activate $I_{Na(W)}$. Within 1 min of exposing the cells to CRS (30 or 100 µM), the magnitude (i.e., ∆area) was strikingly decreased due to the 50-ms ascending V_{ramp} (**Figure 3**). For example, exposure to 30 or 100 µM CRS led to considerable attenuation of the ∆area of $I_{Na(W)}$ from a control value of 4.43 ± 0.58 mV·nA (*n* = 7) to 2.91 ± 0.51 mV·nA (*n* = 7, *p* < 0.05) or 1.86 ± 0.47 mV·nA (*n* = 7, *p* < 0.05), respectively. Deltamethrin (DLT), a type II pyrethroid, was reported to activate I_{Na} (Bothe and Lampert, 2021). Under continuous exposure to 100 µM CRS, the exposure of cells to 10 µM DLT effectively increased the ∆area to 3.15 ± 0.54 mV·nA (*n* = 7, *p* < 0.05), indicating that CRS-mediated increase in $I_{Na(W)}$ can be partially restored by further addition of DLT. Our results also confirm that CRS primarily inhibits $I_{Na(W)}$ itself, rather than other types of voltage-gated ionic currents.

3.4. CRS-mediated increase in the cumulative inhibition of $I_{Na(T)}$ inactivation

$I_{Na(T)}$ inactivation was recently shown to accumulate during repetitive short pulses, and this accumulation is thought to be responsible for various electrical behaviors (Huang et al., 2015; Navarro et al., 2020). Therefore, an additional series of measurements was performed to ascertain whether CRS could perturb $I_{Na(T)}$ inactivation following activation by a train of
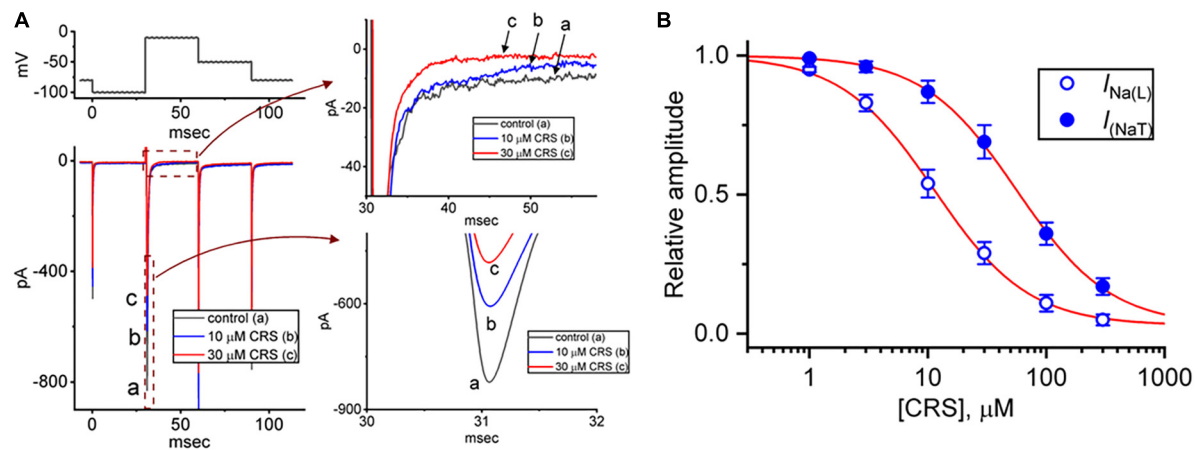
FIGURE 1
Inhibitory effects of carisbamate (CRS) on the transient (peak, $I_{Na(T)}$) or late (sustained, $I_{Na(L)}$) component of the voltage-gated Na$^+$ current (I_{Na}).
(A) The exemplar current traces shown at left were acquired in the control period without CRS (a, black line) and during exposure to 10 μM (b, blue line) or 30 μM CRS (c, red line). The voltage-clamp protocol is illustrated at the top left, while the current traces shown at right represent expansions of the records from the dashed boxes in the left side of panel **(A)**. **(B)** Concentration-dependent CRS-induced inhibition of $I_{Na(T)}$ (filled blue circles) and $I_{Na(L)}$ (open blue circles) in GH$_3$ cells. Each data point indicates the mean ± standard error of the mean ($n = 8$). The red sigmoidal lines, on which the data points are overlaid, indicate the best fit to a modified Hill equation according to the averaged data obtained at each concentration of CRS, as elaborated in the section "2. Materials and methods". The IC$_{50}$ values required for CRS-mediated inhibition of $I_{Na(T)}$ and $I_{Na(L)}$ were 56.4 and 11.4 μM, respectively.
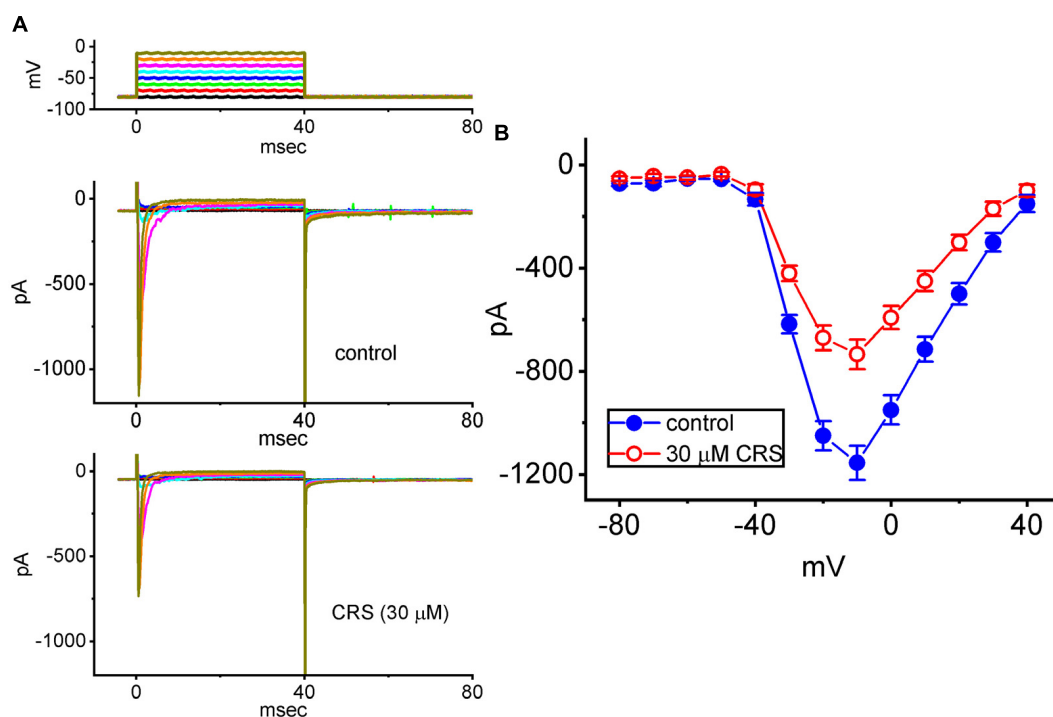

FIGURE 2
Inhibitory effect of CRS on the steady-state current versus voltage ($I-V$) relationship of the transient peak component of the voltage-gated Na$^+$ current ($I_{Na(T)}$). **(A)** Exemplar current traces acquired in pituitary GH$_3$ cells in the control period without CRS (upper) and during exposure to 30 μM CRS (lower). The voltage-clamp protocol is illustrated at the top, and the potential traces shown in different colors correspond to the current traces evoked by the same levels of step commands. **(B)** Averaged $I-V$ relationships of $I_{Na(T)}$ acquired in the absence (blue filled circles) and presence (red open circles) of 30 μM CRS. Each point represents the mean ± standard error of the mean ($n = 8$). The current amplitude was obtained at the beginning of each depolarization step from a holding potential of −80 mV.

depolarizing stimuli. The studied cell was held at a voltage of −80 mV and subjected to the following stimulus protocol: repetitive depolarization from −10 mV (40 ms per pulse at a rate of 20 Hz for 1 s). $I_{Na(T)}$ inactivation in GH$_3$ cells was evoked by 1-s repetitive depolarization from −80 to −10 mV with a decay time constant of 56.4 ± 5.6 ms ($n = 7$), which was obtained

FIGURE 3

Modification by carisbamate (CRS) of a nonlinear window I_{Na} ($I_{Na(W)}$) in response to a short ascending ramp voltage (V_{ramp}). **(A)** Exemplar current traces (i.e., the relationship of current amplitude versus non-linear membrane potential) obtained in the control period without CRS (a, black) and during exposure to 30 μM (b, red) or 100 μM CRS (c, blue). The voltage protocol is illustrated in the inset graph; the downward deflection denotes the instantaneous inward current (i.e., $I_{Na(W)}$) activated by a short ascending V_{ramp}. **(B)** Bar graph summarizing the effect of CRS (30 or 100 μM) and CRS (100 μM) plus deltamethrin (DLT, 10 μM) on the Δarea of $I_{Na(W)}$ (mean ± standard error of the mean; $n = 7$ for each bar). The Δarea was measured at voltages between −80 and +40 mV during the ascending V_{ramp}. *Significantly different from the control group ($p < 0.05$), **significantly different from the CRS (30 μM) alone group ($p < 0.05$), and [+]significantly different from the CRS (100 μM) alone group ($p < 0.05$).

during the control period (i.e., absence of CRS) (**Figure 4**). In other words, a rapid current decay occurred as a function of time in a single-exponential manner. In particular, while exposing cells to 10 or 30 μM CRS, the decay time constant of $I_{Na(T)}$ activated by the same train of depolarizing stimuli decreased considerably to 48.3 ± 4.3 ms ($n = 7$, $p < 0.05$) or 31.2 ± 2.8 ms ($n = 7$, $p < 0.05$), respectively. Tel, an antagonist of the angiotensin II receptor, has been recognized as an effective activator of I_{Na} (Chang et al., 2018; Chang and Wu, 2018; Lai et al., 2020). The addition of Tel (10 μM) increased the decay time constant of the current to 40.4 ± 4.5 ms ($n = 7$, $p < 0.05$). Our results confirm that that CRS primarily inhibits Na$^+$ current, which show cumulative inhibition, rather than other type of voltage-gated ionic currents.
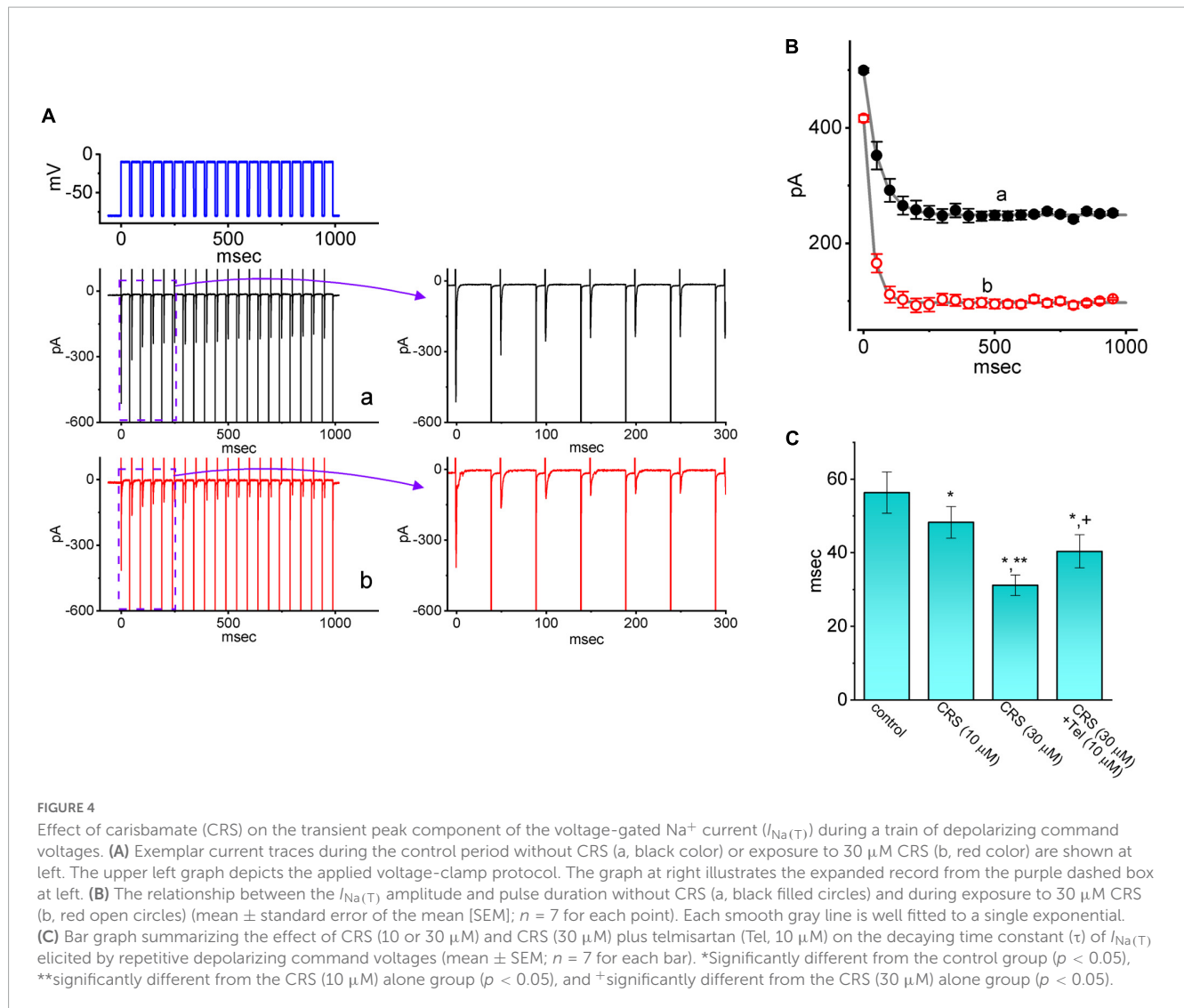
3.5. Attenuating effect of CRS on the DLT-mediated increase in I_{Na}

CRS was shown to effectively modify the magnitude of I_{Na} (Whalley et al., 2009), while DLT was previously reported to be a pyrethroid insecticide that can activate I_{Na} (Bothe and Lampert, 2021; Lin et al., 2022). Therefore, we next investigated whether the presence of CRS could modify the DLT-enhanced I_{Na} evoked in GH$_3$ cells by a rapid depolarizing pulse. In this set of experiments, when establishing whole-cell current recordings, we voltage-clamped the examined cell at −100 mV and applied a 30-ms depolarizing pulse to −10 mV. In keeping with previous observations (Liu Y. et al., 2009; Whalley et al., 2009; Vohora et al., 2010), we found that exposing cells to 10 μM DLT alone for 1 min enhanced the amplitude of $I_{Na(T)}$ or $I_{Na(L)}$ (**Figure 5**). However, the subsequent addition of CRS attenuated this effect of DLT on the depolarization-mediated activation of $I_{Na(T)}$ or $I_{Na(L)}$. For example, as the cells were depolarized from −100 to −10 mV to evoke I_{Na}, exposing the cells to 10 μM DLT resulted

in a considerable increase in $I_{Na(T)}$ or $I_{Na(L)}$ from a control value of 412 ± 14 pA ($n = 8$) or 89 ± 9 pA ($n = 8$), respectively, to 607 ± 18 pA ($n = 8$, $p < 0.05$) or 178 ± 13 pA ($n = 8$, $p < 0.05$), respectively. Moreover, the further addition of 10 μM CRS to the cells, which remained under continuous exposure to DLT, greatly reduced $I_{Na(T)}$ or $I_{Na(L)}$ to 478 ± 15 pA ($n = 8$, $p < 0.05$) or 141 ± 11 pA ($n = 8$, $p < 0.05$), respectively. In this regard, the experimental data reflect that CRS could modify the DLT-mediated enhancement of the magnitude of $I_{Na(T)}$ and $I_{Na(L)}$ in GH$_3$ cells.

3.6. Effect of CRS on the amplitude of the hyperpolarization-activated cation current (I_h) in GH$_3$ cells

We further investigated the effects of CRS and other relevant compounds on I_h. In these experiments, we placed cells in Ca^{2+}-free Tyrode's solution and filled the recording electrode with a K$^+$-enriched solution. We then applied long-lasting step hyperpolarization to activate an inwardly directed current with slowly activating and deactivating properties. Studies have identified this type of ionic current as the I_h or I_f (**Figure 6A**) (Belardinelli et al., 1988; Irisawa et al., 1993; Simasko and Sankaranarayanan, 1997; Liu Y. C. et al., 2009; Wu et al., 2022b; Chuang et al., 2022). Within 1 min of exposing the GH$_3$ cells to CRS (10 or 30 μM), the I_h amplitude in response to such membrane hyperpolarization exhibited an evident decrease. For example, as the cells were hyperpolarized from −40 to −110 mV for a duration of 2 s, exposure to CRS at 10 or 30 μM noticeably reduced the amplitude of the late inward current at the end of hyperpolarization from a control value of 136 ± 18 pA ($n = 8$) to 103 ± 17 pA ($n = 8$, $p < 0.05$) or 73 ± 12 pA ($n = 8$, $p < 0.05$), respectively. Upon returning to −40 mV, the amplitude of the deactivating I_h decreased from a control value of 93 ± 13 pA ($n = 8$) to 73 ± 12 pA

FIGURE 4

Effect of carisbamate (CRS) on the transient peak component of the voltage-gated Na$^+$ current ($I_{Na(T)}$) during a train of depolarizing command voltages. **(A)** Exemplar current traces during the control period without CRS (a, black color) or exposure to 30 μM CRS (b, red color) are shown at left. The upper left graph depicts the applied voltage-clamp protocol. The graph at right illustrates the expanded record from the purple dashed box at left. **(B)** The relationship between the $I_{Na(T)}$ amplitude and pulse duration without CRS (a, black filled circles) and during exposure to 30 μM CRS (b, red open circles) (mean ± standard error of the mean [SEM]; n = 7 for each point). Each smooth gray line is well fitted to a single exponential. **(C)** Bar graph summarizing the effect of CRS (10 or 30 μM) and CRS (30 μM) plus telmisartan (Tel, 10 μM) on the decaying time constant (τ) of $I_{Na(T)}$ elicited by repetitive depolarizing command voltages (mean ± SEM; n = 7 for each bar). *Significantly different from the control group ($p < 0.05$), **significantly different from the CRS (10 μM) alone group ($p < 0.05$), and $^+$significantly different from the CRS (30 μM) alone group ($p < 0.05$).

(n = 8, $p < 0.05$) or 51 ± 9 pA (n = 8, $p < 0.05$) under exposure to 10 or 30 μM CRS, respectively. As shown in **Figure 6A**, the activation time constant (τ_{act}) of I_h elicited during long membrane hyperpolarization also increased, as evidenced by a significant rise in the τ_{act} value from 212 ± 12 to 402 ± 19 m (n = 8, $p < 0.05$) in the presence of 30 μM CRS. This suppression of I_h in GH$_3$ cells was readily reversed upon the removal of CRS.

The relationship between the concentration of CRS and the relative amplitude of I_h is illustrated in **Figure 6B**. Exposure to CRS was found to reduce the amplitude of I_h during long membrane hyperpolarization in a concentration-dependent manner. Using the modified Hill equation, the IC$_{50}$ value required for CRS to inhibit the I_h amplitude as seen in GH$_3$ cells was estimated to be 38 μM; 1 mM CRS almost completely inhibited the current amplitude.

We further studied the average I–V relationship for I_h in the presence or absence of 30 μM CRS. As shown in **Figures 7A, B**, this I–V relationship exhibited robust, inwardly rectifying non-ohmic behavior. Under exposure to CRS, the I_h amplitude in the cells was depressed throughout the voltage clamp step. For example, CRS exposure markedly decreased the whole-cell I_h conductance,

measured between −120 and −100 mV, from 6.9 ± 0.2 to 5.3 ± 0.2 nS (n = 8, $p < 0.05$); after washout of CRS, the I_h conductance was restored to 6.7 ± 0.2 nS (n = 7, $p < 0.05$).

3.7. Suppressive effect of CRS on the voltage-dependent hysteresis (Hys$_{(V)}$) of I_h evoked in response to a long-lasting triangular V_{ramp}

The Hys$_{(V)}$ behavior of I_h has been shown to strongly influence electrical behaviors (i.e., action potential firing) in different types of excitable cells (Männikkö et al., 2005; Fürst and D'Alvanzo, 2015; Chan et al., 2020; Chuang et al., 2022; Wu et al., 2022b). For this reason, we explored whether CRS could perturb the Hys$_{(V)}$ behavior of I_h. In this stage of whole-cell experiments, we applied a long-lasting inverted triangular V_{ramp} for a duration of 2 s (i.e., with a ramp pulse of ±40 mV/s) to measure the Hys$_{(V)}$ properties. As shown in **Figure 8**, the trajectory of I_h activation in response to the downsloping (i.e., hyperpolarization from −40 to −120 mV) and upsloping (depolarization from −120 to −40 mV) limbs of V_{ramp}
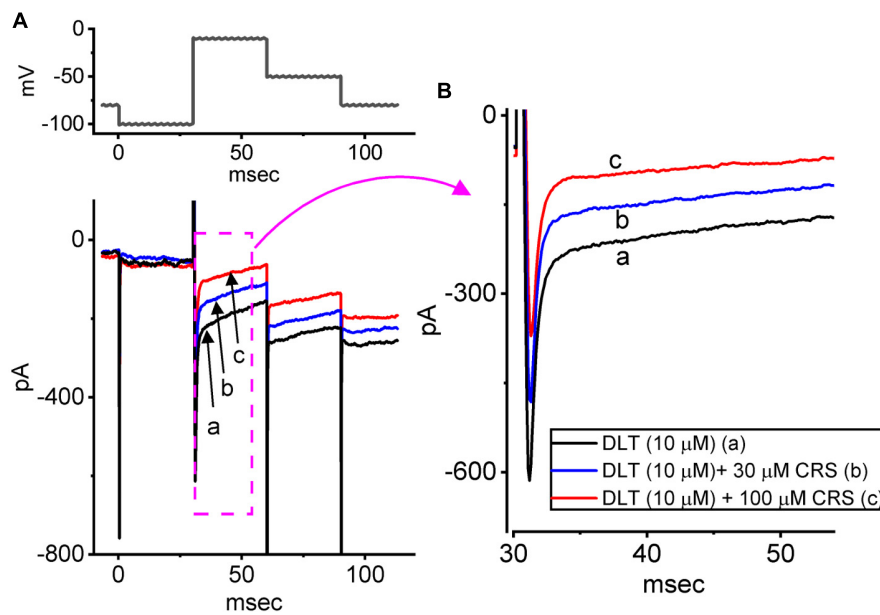
FIGURE 5

Effects of deltamethrin (DLT) alone and plus carisbamate (CRS) on the voltage-gated Na^+ current (I_{Na}). The cells were bathed in Ca^{2+}-free Tyrode's solution containing 10 mM tetraethylammonium chloride and 0.5 mM $CdCl_2$, and the measuring electrode was filled with a Cs^+-enriched solution. **(A)** Exemplar current traces obtained in the presence of DLT (10 μM) alone (a, black), DLT (10 μM) plus CRS (30 μM), or DLT (10 μM) plus CRS (100 μM). **(B)** Expanded records from the pink dashed box in panel **(A)**. Of note, exposure to CRS effectively attenuated DLT-mediated stimulation of $I_{Na(T)}$ and $I_{Na(L)}$ in GH₃ cells.
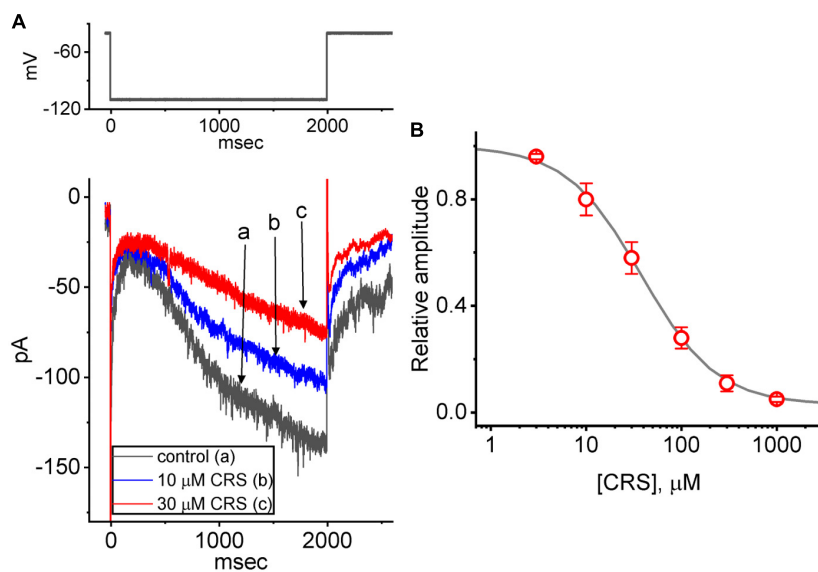
FIGURE 6

Effect of carisbamate (CRS) on the hyperpolarization-activated cation current (I_h). This set of measurements was obtained from cells bathed in Ca^{2+}-free Tyrode's solution containing 1 μM tetrodotoxin, and the measuring electrode was filled with a K^+-enriched solution. **(A)** Exemplar current traces (i.e., I_h) acquired in the control period without CRS (a, black line) and during exposure to 10 μM (b, blue line) or 30 μM CRS (c, red line). The upper graph depicts the applied voltage-clamp protocol. **(B)** Concentration-dependent CRS-mediated suppression of I_h activation via 2-s long-lasting membrane hyperpolarization (mean ± standard error of the mean, $n = 8$ for each point). The gray sigmoidal line, on which the data points are overlaid, indicates the best fit to a modified Hill equation as elaborated in the Materials and methods. The current amplitude was obtained at different CRS concentrations (3 μM–1 mM) at the end of a 2-s period of hyperpolarizing command voltage to −110 mV from a holding potential of −40 mV. The IC_{50} value required for CRS-mediated inhibition of I_h was 38 μM.

as a function of time was distinguishable. The current magnitude in response to the downsloping (descending) limb of the inverted triangular V_{ramp} was much larger than that evoked by the upsloping (ascending) limb. In terms of the relationship between I_h amplitude and membrane potential, we clearly observed the $Hys_{(V)}$ behavior of the current amplitude in a clockwise direction. Interestingly,
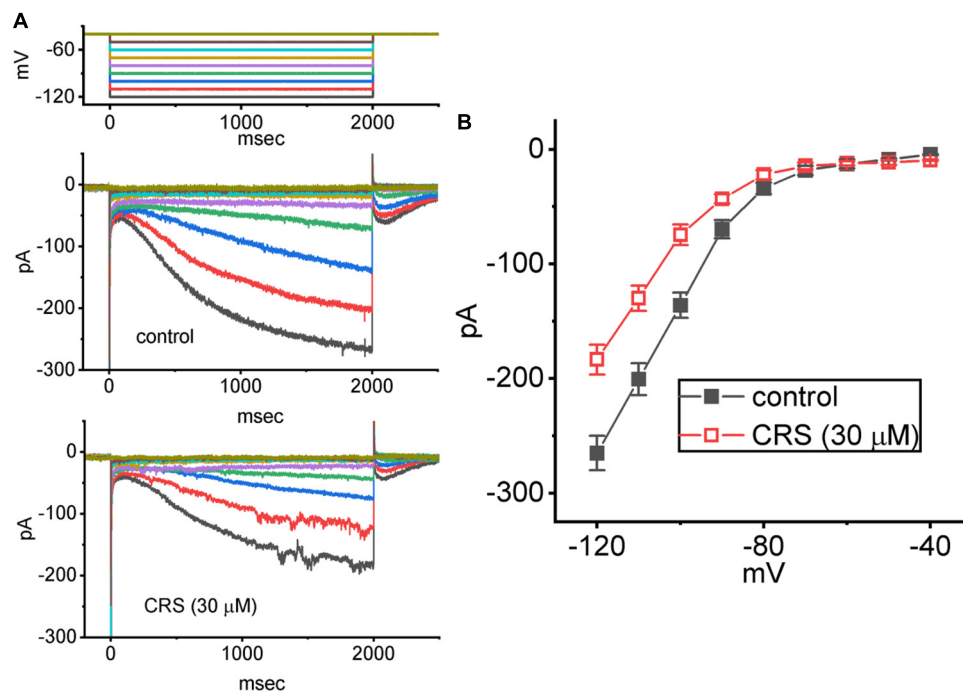
FIGURE 7

Inhibitory effect of carisbamate (CRS) on the average steady-state current versus voltage ($I-V$) relationship of the hyperpolarization-activated cation current (I_h). The cells were bathed in Ca^{2+}-free Tyrode's solution, and a series of 2-s voltage steps between −120 and −40 mV (10 mV per step) was delivered to each studied cell. **(A)** Exemplar current traces obtained in the control period without CRS (upper) and during exposure to 30 μM CRS. The upper graph depicts the voltage-clamp protocol applied to the tested cell. Potential traces shown in different colors correspond to the ionic currents that were evoked by the same level of command voltage. **(B)** Average $I-V$ relationship of I_h acquired in the absence (filled black squares) and presence (open red squares) of 30 μM CRS (mean ± standard error of the mean; $n = 8$ for each point). The current amplitude was measured at the end of each voltage step with a duration of 2 s.

when the GH$_3$ cells were continually exposed to CRS, the Hys$_{(V)}$ strength of I_h evoked by the inverted triangular V_{ramp} progressively decreased (**Figure 8**). For example, the strength (i.e., Δarea) of V_{ramp}-induced I_h in the control period (i.e., absence of CRS) was 4.16 ± 0.31 mV·nA ($n = 8$). However, after exposure to 10 or 30 μM CRS for 1 min, the value of Hys$_{(V)}$'s Δarea in GH$_3$ cells was reduced significantly to 3.24 ± 0.25 mV·nA ($n = 8$, $p < 0.05$) or 2.92 ± 0.22 mV·nA ($n = 8$, $p < 0.05$), respectively. OXAL, a chemotherapeutic drug, has been shown to activate I_h (Resta et al., 2018; Chang et al., 2020; Yongning et al., 2021). In cells exposed continuously to 30 μM CRS, the subsequent application of OXAL (10 μM) reversed the CRS-mediated decrease in the Δarea to 4.23 ± 0.28 mV·nA ($n = 8$, $p < 0.05$).

3.8. Predicted docking interaction of the CRS molecule with the HCN channel

We wanted to study how CRS could interact with the HCN channel protein, but since it is not known so far the isoform(s) blocked by the CRS, we have used the structure of a closely related CNG (cyclic nucleotide-gated) channel. Information from the provider of the original structure data from PDB (James et al., 2017) revealed several close relationships between the cryostructure of CNG and HCN. The CNG channel protein structure was obtained from PDB (PDB ID: 5V4S); we used PyRx software to see how the CRS molecule could dock into the channel protein.

Figure 9 presents the predicted docking sites of CRS for interaction with amino acid residues of the CNG channel. Specifically, the CRS molecule was predicted to form hydrophobic contacts with the CNG channel residues Ala232(A), Ala232(B), Ala232(C), Ser233(A) Ser233(B), Gly236(C), Gly236(D), and Ser237(D), as well as hydrogen bonds with residues Ala232(D) and Ser232(C), with estimated distances of 3.15 and 3.05 Å, respectively. It is likely that the CRS molecule interacts with the transmembrane region (position 211–238) or membrane segment (position 210–235 or 211–231) of the CNG channel, although details of these binding sites remain unclear. Moreover, as shown in **Supplementary Figure 1**, the docking interaction of the CRS molecule with the hNa$_V$1.7 channel was generated in the Supplementary information.

4. Discussion

The current study has yielded several main findings. First, CRS can exert the inhibitory effect on I_{Na} which can vary depending on the concentration applied, time course of the current, and stimulus frequency used. Second, exposure to CRS led to differential suppression of $I_{Na(T)}$ and $I_{Na(L)}$ activation in response to a brief step depolarization, with effective IC$_{50}$ values of 56.4 and 11.4 μM, respectively. Third, CRS failed to alter the steady-state $I-V$ relationship of $I_{Na(T)}$ in GH$_3$ cells but decreased the decay time constant of cumulative $I_{Na(T)}$ inactivation during pulse train stimulation. Fourth, DLT-mediated enhancement of I_{Na} was
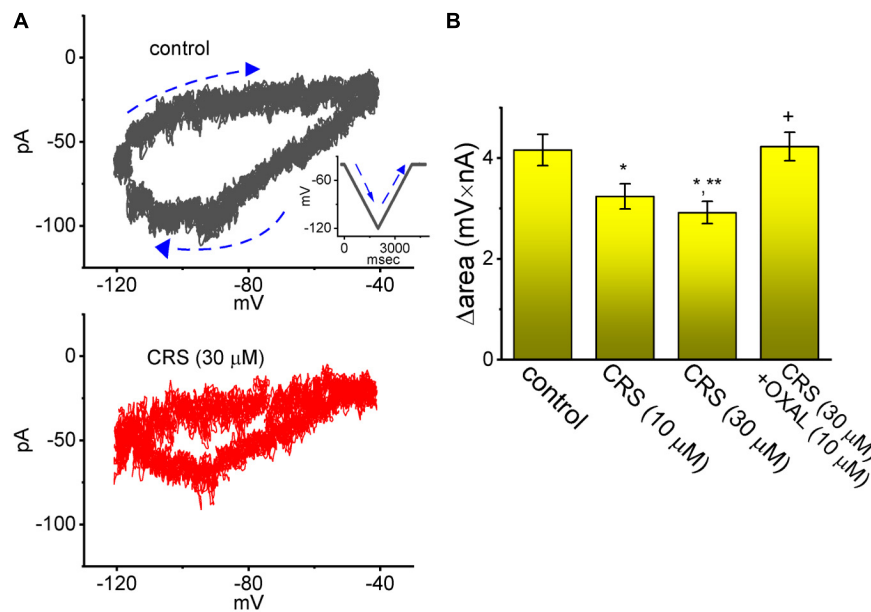
FIGURE 8

Attenuating effect of carisbamate (CRS) on the voltage-dependent hysteresis ($Hys_{(V)}$) of the hyperpolarization-activated cation current (I_h). **(A)** Exemplar $Hys_{(V)}$ (i.e., current trace versus ramp voltage [V_{ramp}]) acquired in the absence (upper graph, gray line) and presence (lower graph, red line) of 30 μM CRS. The inset in the upper graph depicts the applied V_{ramp} protocol. Dashed arrows show the direction of I_h or the voltage trace in which time passes during the elicitation of an inverted triangular V_{ramp}. **(B)** Bar graph summarizing the effects of CRS (10 or 30 μM) and CRS (30 μM) plus oxaliplatin (OXAL, 10 μM) on the Δarea of the $Hys_{(V)}$ of I_h (mean $\pm$ standard error of the mean; $n = 8$ for each yellow bar). The Δarea, indicated as a function of the strength of the window component of the voltage-gated Na^+ current ($I_{Na(W)}$), was calculated under the encircled area, which was activated during the downsloping (descending) and upsloping (ascending) ends of the triangular V_{ramp}. Note the V_{ramp}-induced $Hys_{(V)}$ for I_h elicitation; the strength of this $Hys_{(V)}$ was attenuated by adding CRS. *Significantly different from the control group ($p < 0.05$), **significantly different from the CRS (10 μM) alone group ($p < 0.05$), and +significantly different from the CRS (30 μM) alone group ($p < 0.05$).
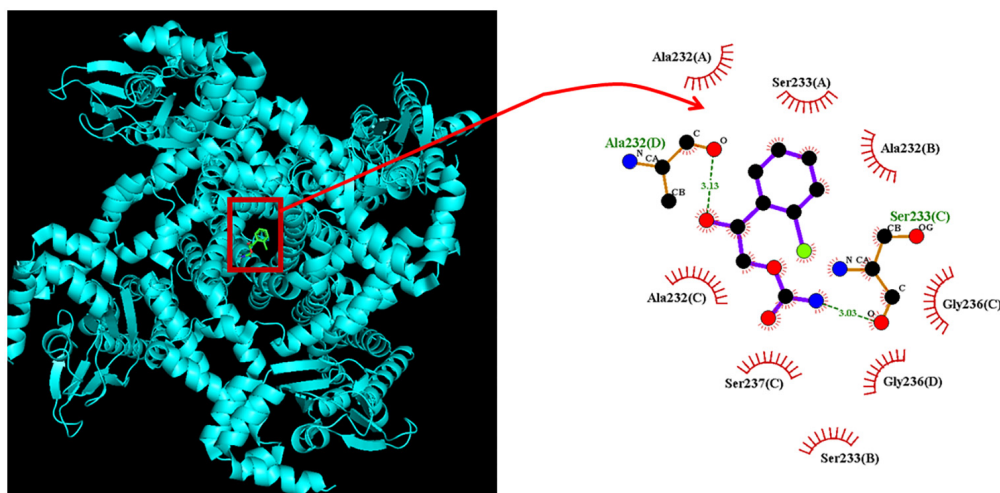

FIGURE 9

Predicted docking between the CNG (cyclic nucleotide-gated) channel and the carisbamate (CRS) molecule. **(Left panel)** Depicts the CNG channel protein structure acquired from RCSB PDB (PDB ID: 5V4S) and the CRS molecular structure acquired from PubChem (Compound CID: 6918474). PyRx software (https://pyrx.sourceforge.io/) (accessed on 28 April 2023) was used to show that the HCN channel structure can be properly docked by the CRS molecule. **(Right panel)** Depicts an expansion of the red box in the **left panel** arrow. This diagram of the interaction between the CNG channel and the CRS molecule was generated using LigPlot+ (https://www.ebi.ac.uk/thornton-srv/software/LIGPLOT/) (accessed on 28 April 2023). The red arcs over which spokes radiate toward the ligand (i.e., CRS) represent hydrophobic contacts, while the green dotted lines indicate hydrogen bond formation. The graph in the **right panel** indicates an expanded display of red box with a curve arrow in the left side.

attenuated by subsequent exposure to CRS. Fifth, CRS elicited a concentration-dependent decrease in I_h amplitude, with an IC_{50} value of 38 μM. Sixth, CRS suppressed the $Hys_{(V)}$ strength of I_h

activation in response to a long-lasting isosceles-triangular V_{ramp}. Collectively, these results demonstrate that CRS-mediated changes in the magnitude, gating properties, and frequency dependence

of I_{Na} and in the magnitude of I_h and $Hys_{(V)}$ can modify the functional activities of electrically excitable cells.

The IC_{50} value required for CRS-mediated inhibition of $I_{Na(T)}$ or $I_{Na(L)}$ was lower than the concentration used to suppress the evoked action potentials in previous studies of piriform cortical neurons or hippocampal neurons (Liu Y. et al., 2009; Whalley et al., 2009). Unlike a previous report showing inability of CRS to alter $I_{Na(L)}$ measured from rat hippocampal neurons (Liu Y. et al., 2009), the IC_{50} value required for CRS-mediated inhibition of $I_{Na(T)}$ in rat hippocampal neurons was estimated to be around 100 µM (Liu Y. et al., 2009), which is greater than the IC_{50} values that we estimated for the suppression of $I_{Na(T)}$ or $I_{Na(L)}$. Therefore, during cell exposure to CRS at pharmacologically achievable concentrations, it is plausible to assume that CRS-induced inhibition of I_{Na} is an important ionic mechanism underlying the perturbing effects of the drug on membrane excitability.

In this study, the exponential decline of $I_{Na(T)}$ during a 20-Hz train of depolarizing pulses (i.e., 40-ms depolarizing pulses from −80 to −10 mV at 20 Hz for 1 s) became pronounced with exposure to CRS. The results reflect the frequency dependence of $I_{Na(T)}$ during pulse train stimulation, consistent with recent studies (Huang et al., 2015; Navarro et al., 2020; Wu et al., 2022a). As a result, exposure to CRS would lead to a loss of function due to changes in the time-dependent current inactivation. Therefore, the CRS-mediated decrease in $I_{Na(T)}$ is closely linked to the strong frequency-dependent decrease in $I_{Na(T)}$ during pulse train stimulation (Navarro et al., 2020).

An earlier report showed that CRS could suppress the magnitude of a T-type Ca^{2+} current (Kim et al., 2017). Therefore, we postulated that in GH_3 cells, a CRS-induced block of I_{Na} could be due, in part, to the inhibitory effect of the drug on the voltage-gated Ca^{2+} currents that are functionally expressed in excitable cells (Wu et al., 2003; Stojilkovic et al., 2010). However, under our experimental conditions, the voltage-gated inward currents were either sensitive to stimulation by Tel and DLT or were suppressed by TTX. Tel and DLT were previously shown to activate I_{Na} (Chang and Wu, 2018; Lai et al., 2020; Bothe and Lampert, 2021; Lin et al., 2022), while TTX is a potent inhibitor of I_{Na}. Under continuous exposure to CRS, exposure to DLT strikingly counteracted the CRS-induced decrease in the instantaneous $I_{Na(W)}$ in GH_3 cells, and exposure to Tef reversed the CRS-mediated reduction of the decaying time constant of $I_{Na(T)}$ inactivation in response to PT depolarizing stimuli. Alternatively, neither $CdCl_2$ nor nimodipine effectively inhibited the inward currents in GH_3 cells. These results prompt us to reflect that, I_{Na} ($I_{Na(T)}$, $I_{Na(L)}$ and $I_{Na(W)}$) is susceptible to blockade by CRS, and that this drug exerts stronger suppressive effects on $I_{Na(L)}$ than on $I_{Na(T)}$. The action of CRS on excitable membranes cannot be explained solely by its ability to suppress the magnitude of a T-type Ca^{2+} current.

CRS was shown to increase Cl^- conductance in piriform cortical neurons (Whalley et al., 2009). In our study, the I_h amplitude was not inhibited by chlorotoxin (1 µM) but was inhibited by ivabradine (10 µM) (data not shown). Similarly, chlorotoxin did not suppress the amplitude of $I_{Na(T)}$ or $I_{Na(L)}$ in tested cells. Chlorotoxin is known to suppress Cl^- channels. It is therefore tempting to speculate that CRS-induced inhibition of I_{Na} or I_h is not associated with an increase in Cl^- channel activity.

In this study, exposure to CRS led to a change in I_h in a concentration-dependent manner, with an IC_{50} value of 38 µM.

There also was a marked retardation of the activation time course (i.e., an increase in the τ_{act} value) of I_h in response to a 2-s hyperpolarizing command voltage. Increasing evidence suggests that the strength of non-equilibrium $Hys_{(V)}$ in V_{ramp}-evoked I_h plays an essential role in modifying electrical behavior (e.g., action potential firing) in various types of excitable cells (Männikkö et al., 2005; Fürst and D'Alvanzo, 2015; Peters et al., 2021, 2022; Wu et al., 2022b). In our study, exposure to CRS also suppressed the $Hys_{(V)}$ of I_h activation during the triangular V_{ramp}, indicating that this drug is likely to interact with the voltage-sensing domains of the HCN channel.

There are four mammalian isoforms of HCN, namely HCN1, HCN2, HCN3, and HCN4, which constitute the macroscopic I_h (or I_f) (Fürst and D'Alvanzo, 2015; Peters et al., 2022). HCN2, HCN3, and mixed HCN2+HCN3 channels are abundantly expressed in GH_3 cells and other types of endocrine and neuroendocrine cells (Kretschmannova et al., 2006, 2012). We emphasize that I_h has been demonstrated to be functionally present in heart cells (Belardinelli et al., 1988; Irisawa et al., 1993; Depuydt et al., 2022). Therefore, the CRS-mediated inhibition of I_h seen in excitable cells is very likely to be responsible for the drug's ability to attenuate an increase in heart rate induced by exposure to organophosphate administration, as described previously (Deshpande et al., 2016a,b; Deshpande and DeLorenzo, 2020). Apart from the ability of CRS to inhibit I_{Na}, as detailed above, CRS-mediated changes in the magnitude, gating kinetics, and $Hys_{(V)}$ behavior of I_h also may be of pharmacological or therapeutic relevance.

In dendritic synapses, I_h has a shunt mechanism that paces the excitatory post-synaptic potential amplitude and duration and limits temporal summation (Magee, 1998, 1999). HCN2 is strongly expressed in the thalamus, where it is involved in the spontaneous firing of thalamocortical neurons in oscillation or in the 3-Hz spike and wave pattern (Poolos, 2004). A study of human subjects revealed a role for HCN2 in susceptibility to juvenile myoclonic epilepsy (Wu et al., 2018). HCN2-knockout animals have been reported to develop spontaneous absence seizures and cardiac sinus arrhythmia (Poolos, 2004; Heuermann et al., 2016). Dendritic HCN1 and HCN2 channels were found to be downregulated in a pilocarpine model of epilepsy, while in the chronic period, expression of these channels increased (Jung et al., 2007). The differential regulation of I_h in different seizure models suggests that a region-specific density of I_h may serve various purposes in epileptogenesis and may play a role in protection against or resistance to seizures. Furthermore, an increased I_h may co-exist with, and possibly contribute to, persistent dendritic hyperexcitability following febrile seizures in the hippocampus, in contrast to the exclusively anti-convulsive role often attributed to an increased I_h (Dyhrfjeld-Johnsen et al., 2008). Interestingly, the inhibitory action of I_h may be caused by its interaction with the delayed-rectifier M-type K^+ current, which can enhance or inhibit spike firing in response to an excitatory post-synaptic potential when the spike threshold is low or high, respectively (George et al., 2009). Additionally, the coupling of I_h to A-type K^+ channels was shown to regulate neuronal excitability (Mishra and Narayanan, 2015). Further studies are needed to clarify the concerted effects of CRS on I_h and I_{Na} in epileptogenesis.

Finally, the modulatory actions of CRS on ion channels demonstrated in this report are not limited to the interactions of this drug with Na_V channels. The inhibitory effects of CRS

on $I_{Na(T)}$, $I_{Na(L)}$, $I_{Na(W)}$, and I_h are also expected to constitute important underlying mechanisms through which the drug exerts concerted effects on cellular function and excitability.

Data availability statement

The original contributions presented in this study are included in the article/Supplementary material, further inquiries can be directed to the corresponding authors.

Author contributions

T-YH, S-NW, and C-WH designed the experiment, analyzed the data, and wrote the manuscript. S-NW and C-WH performed the experiments and created the figures. All authors contributed to the article and approved the submitted version.

Funding

Acknowledgments

Conflict of interest

The authors declare that the research was conducted in the absence of any commercial or financial relationships that could be construed as a potential conflict of interest.

Publisher's note

All claims expressed in this article are solely those of the authors and do not necessarily represent those of their affiliated organizations, or those of the publisher, the editors and the reviewers. Any product that may be evaluated in this article, or claim that may be made by its manufacturer, is not guaranteed or endorsed by the publisher.

Supplementary material

The Supplementary Material for this article can be found online at: https://www.frontiersin.org/articles/10.3389/fncel.2023.1159067/full#supplementary-material

References

Anastasaki, C., Mo, J., Cehn, J. K., Chatterjee, J., Pan, Y., Scheaffer, S. M., et al. (2022). Neuronal hyperexcitability drives central and peripheral nervous system tumor progression in models of neurofibromatosis-1. *Nat. Commun.* 13:2785. doi: 10.1038/s41467-022-30466-6

Banarroch, E. E. (2013). HCN channels: function and clinical implications. *Neurology* 80, 304–310. doi: 10.1212/WNL.0b013e31827dec42

Belardinelli, L., Giles, W. R., and West, A. (1988). Ionic mechanisms of adenosine actions in pacemaker cells from rabbit heart. *J. Physiol.* 405, 615–633. doi: 10.1113/jphysiol.1988.sp017352

Bothe, S. N., and Lampert, A. (2021). The insecticide deltamethrin enhances sodium channel slow inactivation of human Nav1.9, Nav1.8 and Nav1.7. *Toxicol. Appl. Pharmacol.* 428:115676. doi: 10.1016/j.taap.2021.115676

Cao, Y., Pang, J., and Zhou, P. (2016). HCN channel as therapeutic targets for heart failure and pain. *Curr. Top. Med. Chem.* 16, 1855–1861. doi: 10.2174/1568026616666151215104058

Catterall, W. A., Lenaeus, M. J., and Gamal El-Din, T. M. (2020). Structure and pharmacology of voltage-gated sodium and calcium channels. *Annu. Rev. Pharmacol. Toxicol.* 60, 133–154. doi: 10.1146/annurev-pharmtox-010818-021757

Chan, M. H., Chen, H. H., Lo, Y. C., and Wu, S. N. (2020). Effectiveness in the block by honokiol, a dimerized allylphenol from Magnolia officinalis, of hyperpolarization-activated cationic current and delayed-rectifier K$^+$ current. *Int. J. Mol. Sci.* 21:4260. doi: 10.3390/ijms21124260

Chang, T. T., Yang, C. J., Lee, Y. C., and Wu, S. N. (2018). Stimulatory action of telmisartan, an antagonist of angiotensin II receptor, on voltage-gated Na$^+$ current: experimental and theoretical studies. *Chin. J. Physiol.* 61, 1–13. doi: 10.4077/CJP.2018.BAG516

Chang, W. T., Gao, Z. H., Li, S. W., Liu, P. Y., Lo, Y. C., and Wu, S. N. (2020). Characterization in dual activation by oxaliplatin, a platinum-based chemotherapeutic agent of hyperpolarization-activated cation and electroporation-induced currents. *Int. J. Mol. Sci.* 21:396. doi: 10.3390/ijms21020396

Chang, W. T., and Wu, S. N. (2018). Activation of voltage-gated sodium current and inhibition of erg-mediated potassium current caused by telmisartan, an antagonist of angiotensin II type-1 receptor, in HL-1 atrial cardiomyocytes. *Clin. Exp. Pharmacol. Physiol.* 45, 797–807. doi: 10.1111/1440-1681.12943

Choi, K., Yi, J. H., Lee, C., Park, K., Kang, S. J., and Shin, K. S. (2022). Presynaptic HCN channel activity is required for the expression of long-term potentiation at lateral amygdala to basal amygdala synapses. *Biochem. Biophys. Res. Commun.* 637, 100–107. doi: 10.1016/j.bbrc.2022.11.020

Chuang, C. W., Chang, K. P., Cho, H. Y., Chuang, T. H., Yu, M. C., Wu, C. L., et al. (2022). Characterization of inhibitory capability on hyperpolarization-activated cation current caused by lutein (β,ε-carotene-3,3-diol), a dietary xanthophyll carotenoid. *Int. J. Mol. Sci.* 23:7186. doi: 10.3390/ijms23137186

Concepcion, F. A., Khan, M. N., Ju Wang, J. D., Wei, A. D., Ojemann, J. G., Ko, A. L., et al. (2021). HCN channel phosphorylation sites mapped by mass spectrometry in human epilepsy patients and in an animal model of temporal lobe epilepsy. *Neuroscience* 460, 13–30. doi: 10.1016/j.neuroscience.2021.01.038

Depuydt, A. S., Peigneur, S., and Tytgat, J. (2022). Review: HCN channels in the heart. *Curr. Cardiol. Rev.* 18:e040222200836.

Deshpande, L. S., Blair, R. E., Huang, B. A., Phillips, K. F., and DeLorenzo, R. J. (2016a). Pharmacological blockade of the calcium plateau provides neuroprotection following organophosphate paraoxon induced status epilepticus in rats. *Neurotoxicol. Teratol.* 56, 81–86. doi: 10.1016/j.ntt.2016.05.002

Deshpande, L. S., Blair, R. E., Phillips, K. F., and DeLorenzo, R. J. (2016b). Role of the calcium plateau in neuronal injury and behavioral morbidities following organophosphate intoxication. *Ann. N. Y. Acad. Sci.* 1374, 176–183. doi: 10.1111/nyas.13122

Deshpande, L. S., and DeLorenzo, R. J. (2020). Novel therapeutics for treating organophosphate-induced status epilepticus co-morbilities, based on changes in calcium homeostasis. *Neurobiol. Dis.* 133:104418. doi: 10.1016/j.nbd.2019.03.006

Deshpande, L. S., Nagarkatti, N., Sombati, S., and DeLorenzo, R. J. (2008a). The novel antiepileptic drug carisbamate (RWJ 333369) is effective in inhibiting spontaneous recurrent seizure discharges and blocking sustained repetitive firing in cultured hippocampal neurons. *Epilepsy Res.* 79, 158–165. doi: 10.1016/j.eplepsyres.2008.01.002

Deshpande, L. S., Nagarkatti, N., Ziobro, J. M., Sombati, S., and DeLorenzo, R. J. (2008b). Carisbamate prevents the development and expression of spontaneous recurrent epileptiform discharges and is neuroprotective in cultured hippocampal neurons. *Epilepsia* 49, 1795–1802. doi: 10.1111/j.1528-1167.2008.01667.x

Dyhrfjeld-Johnsen, J., Morgan, R. J., Földy, C., and Soltesz, I. (2008). Upregulated H-current in hyperexcitable CA1 dendrites after febrile seizures. *Front. Cell. Neurosci.* 2:2. doi: 10.3389/neuro.03.002.2008

Elkommos, S., and Mula, M. (2022). Current and future pharmacotherapy options for drug-resistant epilepsy. *Expert Opin. Pharmacother.* 23, 2023–2034. doi: 10.1080/14656566.2022.2128670

Faure, J. B., Akimana, G., Carneiro, J. E., Cosquer, B., Ferrandon, A., Geiger, K., et al. (2013). A comprehensive behavioral evaluation in the lithium-pilocarpine model in rats: effects of carisbamate administration during status epilepticus. *Epilepsia* 54, 1203–1213. doi: 10.1111/epi.12219

Faure, J. B., Marques-Carneiro, J. E., Akimana, G., Cosquer, B., Ferrandon, A., Herbeaux, K., et al. (2014). Attention and executive functions in a rat model of chronic epilepsy. *Epilepsia* 55, 644–653. doi: 10.1111/epi.12549

Fernandes, M. J., Carneiro, J. E., Amorim, R. P., Araujo, M. G., and Nehlig, A. (2015). Neuroprotective agents and modulation of temporal lobe epilepsy. *Front. Biosci.* 7, 79–93. doi: 10.2741/E719

Fürst, O., and D'Alvanzo, N. (2015). Isoform dependent regulation of human HCN channels by cholesterol. *Sci. Rep.* 5:14270. doi: 10.1038/srep14270

George, M. S., Abbott, L. F., and Siegelbaum, S. A. (2009). HCN hyperpolarization-activated cation channels inhibit EPSPs by interactions with M-type K(+) channels. *Nat. Neurosci.* 12, 577–584. doi: 10.1038/nn.2307

Heuermann, R. J., Jaramillo, T. C., Ying, S. W., Suter, B. A., Lyman, K. A., Han, Y., et al. (2016). Reduction of thalamic and cortical Ih by deletion of TRIP8b produces a mouse model of human absence epilepsy. *Neurobiol. Dis.* 85, 81–92. doi: 10.1016/j.nbd.2015.10.005

Hsiao, H. T., Liu, Y. C., Liu, P. Y., and Wu, S. N. (2019). Concerted suppression of I_h and activation of $I_{K(M)}$ by ivabradine, and HCN channel inhibitor, in pituitary cells and hippocampal neurons. *Brain Res. Bull.* 149, 11–20. doi: 10.1016/j.brainresbull.2019.03.016

Huang, C. W., Hung, T. Y., and Wu, S. N. (2015). The inhibitory actions by lacosamide, a functionalized amino acid, on voltage-gated Na^+ currents. *Neuroscience* 287, 125–136. doi: 10.1016/j.neuroscience.2014.12.026

Hung, T. Y., Wu, S. N., and Huang, C. W. (2021). The integrated effects of brivaracetam, a selective analog of levetiracetam, on ionic currents and neuronal excitability. *Biomedicines* 9:369. doi: 10.3390/biomedicines9040369

Irisawa, H., Brown, H. F., and Giles, W. (1993). Cardiac pacemaking in the sinoatrial node. *Physiol. Rev.* 73, 197–227. doi: 10.1152/physrev

James, Z. M., Borst, A. J., Haitin, Y., Frenz, B., DiMaio, F., Zagotta, W. N., et al. (2017). CryoEM structure of a prokaryotic cyclic nucleotide-gated ion channel. *Proc. Natl. Acad. Sci. U S A.* 114, 4430–4435. doi: 10.1073/pnas.1700248114

Jung, S., Jones, T. D., Lugo, J. N. Jr., Sheerin, A. H., Miler, J. W., D'Ambrosio, R., et al. (2007). Progressive dendritic HCN channelopathy during epileptogenesis in the rat pilocarpine model of epilepsy. *J. Neurosci.* 27, 13012–13021. doi: 10.1523/JNEUROSCI.3605-07.2007

Kim, D. Y., Zhang, F. X., Nakanishi, S. T., Mettler, T., Cho, I. H., Ahn, Y., et al. (2017). Carisbamate blockade of T-type voltage-gated calcium channels. *Epilepsia* 58, 617–626. doi: 10.1111/epi.13710

Kretschmannova, K., Gonzalez-Iglesias, A. E., Tomić, M., and Stojilkovic, S. S. (2006). Dependence of hyperpolarisation-activated cyclic nucleotide-gated channel activity on basal cyclic adenosine monophosphate production in spontaneously firing GH₃ cells. *J. Neuroendocrinol.* 18, 484–493. doi: 10.1111/j.1365-2826.2006.01438.x

Kretschmannova, K., Kucka, M., Gonzalez-Iglesias, A. E., and Stojilkovic, S. S. (2012). The expression and role of hyperpolarization-activate and cyclic nucleotide-gated channels in endocrine anterior pituitary cells. *Mol. Endocrinol.* 26, 153–164. doi: 10.1210/me.2011-1207

Lai, M. C., Wu, S. N., and Huang, C. W. (2020). Telmisartan, an antagonist of angiotensin II receptors, accentuates voltage-gated Na^+ currents and hippocampal neuronal excitability. *Front. Neurosci.* 14:902. doi: 10.3389/fnins.2020.00902

Lai, M. C., Wu, S. N., and Huang, C. W. (2022). Zingerone modulates neuronal voltage-gated Na^+ and L-type Ca^{2+} currents. *Int. J. Mol. Sci.* 23:3123. doi: 10.3390/ijms23063123

Lee, C. Y., Lee, M. L., Shih, C. C., and Liou, H. H. (2011). Carisbamate (RWJ-333369) inhibits glutamate transmission in the granule cell of the dentate gyrus. *Neuropharmacology* 61, 1239–1247. doi: 10.1016/j.neuropharm.2011.07.022

Lei, X., Zeng, J., Yan, Y., and Liu, X. (2022). Blockage of HCN channels inhibits the function of P2X receptors in rat dorsal root ganglion neurons. *Neurochem. Res.* 47, 1083–1096. doi: 10.1007/s11064-021-03509-5

Lin, M. H., Lin, J. F., Yu, M. C., Wu, S. N., Wu, C. L., and Cho, H. Y. (2022). Characterization in potent modulation on voltage-gated Na^+ current exerted by deltamethrin, a pyrethroid insecticide. *Int. J. Mol. Sci.* 23:14733. doi: 10.3390/ijms232314733

Liu, Y., Yohrling, G. J., Wang, Y., Hutchinson, T. L., Brenneman, D. E., Flores, C. M., et al. (2009). Carisbamate, a novel neuromodulator, inhibits voltage-gated sodium channels and action potential firing of rat hippocampal neurons. *Epilepsy Res.* 83, 66–72. doi: 10.1016/j.eplepsyres.2008.09.006

Liu, Y. C., Wang, Y. J., Wu, P. Y., and Wu, S. N. (2009). Tramadol-induced block of hyperpolarization-activated cation current in rat pituitary lactotrophs. *Naunyn-Schmiedeberg's Arch. Pharmacol.* 379, 127–135. doi: 10.1007/s00210-008-0353-0

Löscher, W., Sills, G. J., and White, H. S. (2021). The ups and downs of alkyl-carbamates in epilepsy therapy: how does cenobamate differ? *Epilepsia* 62, 596–614. doi: 10.1111/epi.16832

Lu, C., Zheng, J., Cao, Y., Bresnahan, R., and Martin-McGill, K. J. (2021). Carisbamate add-on therapy for drug-resistant focal epilepsy. *Cochrane Database Syst. Rev.* 12:CD012121. doi: 10.1002/14651858.CD012121.pub2

Magee, J. C. (1998). Dendritic hyperpolarization-activated currents modify the integrative properties of hippocampal CA1 pyramidal neurons. *J. Neurosci.* 18, 7613–7624.

Magee, J. C. (1999). Dendritic Ih normalizes temporal summation in hippocampal CA1 neurons. *Nat. Neurosci.* 2:848. doi: 10.1038/12229

Mäki-Marttunen, T., and Mäki-Marttunen, V. (2022). Excitatory and inhibitory effects of HCN channel modulation on excitability of layer V pyramidal cells. *PLoS Comput. Biol.* 18:e1010506. doi: 10.1371/journal.pcbi.1010506

Männikkö, R., Pandey, S., Larsson, H. P., and Elinder, F. (2005). Hysteresis in the voltage dependence of HCN channels: conversion between two modes affects pacemaker properties. *J. Gen. Physiol.* 125, 305–326. doi: 10.1085/jgp.200409130

Marques-Carneiro, J. E., Persike, D. S., Litzahn, J. J., Cassel, J. C., Nehlig, A., and Fernandes, M. J. D. S. (2017). Hippocampal proteome of rats subjected to the li-pilocarpine epilepsy model and the effect of carisbamate treatment. *Pharmaceuticals (Basel)* 10:67. doi: 10.3390/ph10030067

Menezes, L. F. S., Sabiá Júnior, E. F., Tibery, D. V., Carneiro, L. D. A., and Schwartz, E. F. (2020). Epilepsy-related voltage-gated sodium channelopathies: a review. *Front. Pharmacol.* 11:1276. doi: 10.3389/fphar.2020.01276

Mishra, P., and Narayanan, R. (2015). High-conductance states and A-type K+ channels are potential regulators of the conductance- current balance triggered by HCN channels. *J. Neurophysiol.* 113, 23–43. doi: 10.1152/jn.00601.2013

Morris, C. E., Boucher, P. A., and Joós, B. (2012). Left-shifted nav channels in injured bilayer. Primary targets for neuroprotective nav antagonist? *Front. Pharmacol.* 3:19. doi: 10.3389/fphar.2012.00019

Navarro, M. A., Salari, A., Lin, J. L., Cowan, L. M., Penington, N. J., Milescu, M., et al. (2020). Sodium channels implement a molecular leaky integrator that detects action potentials and regulates neuronal firing. *eLife* 9:e54940. doi: 10.7554/eLife.54940

Noam, Y., Bernard, C., and Baram, T. Z. (2011). Towards an integrated view of HCN channel role in epilepsy. *Curr. Opin. Neurobiol.* 21, 873–879. doi: 10.1016/j.conb.2011.06.013

Ono, T., Moshe, S. L., and Galanopoulou, A. S. (2011). Carisbamate acutely suppresses spasms in a rat model of symptomatic infantile spasms. *Epilepsia* 52, 1678–1684. doi: 10.1111/j.1528-1167.2011.03173.x

Peters, C. H., Liu, P. W., Morotti, S., Gantz, S. C., Brandi, E., Bean, B. P., et al. (2021). Bi-directional flow of the funny current (I_f) during the pacemaking cycle in murine sinoatrial node myocytes. *Proc. Natl. Acad. Sci. U S A.* 118:e2104668118. doi: 10.1073/pnas.2104668118

Peters, C. H., Singh, R. K., Bankston, J. R., and Proenza, C. (2022). Regulation of HCN channels by protein interactions. *Front. Physiol.* 13:928507. doi: 10.3389/fphys.2022.928507

Pong, A. W., Ross, J., Tyrlikova, I., Giermek, A. J., Kohli, M. P., Khan, Y. A., et al. (2022). Epilepsy: expert opinion on emerging drugs in phase 2/3 clinical trials. *Expert Opin. Emerg. Drugs* 27, 75–90. doi: 10.1080/14728214.2022.2059464

Poolos, N. P. (2004). The Yin and Yang of the H-Channel and Its Role in Epilepsy. *Epilepsy Curr.* 4, 3–6. doi: 10.1111/j.1535-7597.2004.04101.x

Resta, F., Micheli, L., Laurino, A., Spinelli, V., Mello, T., Sartiani, L., et al. (2018). Selective HCN block as a strategy to control oxaliplatin-induced neuropathy. *Neuropharmacology* 131, 403–413. doi: 10.1016/j.neuropharm.2018.01.014

Rezvani, A. H., Lawrence, A. J., Arolfo, M. P., Levin, E. D., and Overstreet, D. H. (2012). Novel medication targets for the treatment of alcoholism: preclinical studies. *Recent Pat. CNS Drug Discov.* 7, 151–162. doi: 10.2174/157488912800673182

Rezvani, A. H., Overstreet, D. H., Vaidya, A. H., Zhao, B., and Levin, E. D. (2009). Carisbamate, a novel antiepileptic candidate compound, attenuates alcohol intake in alcohol-preferring rats. *Alcohol. Clin. Exp. Res.* 33, 1366–1373. doi: 10.1111/j.1530-0277.2009.00966.x

Shim, S., El Mansari, M., and Blier, P. (2013). Modulation of the antidepressant-like effects of sustained administration of carisbamate and lamotrigine on monoaminergic systems: electrophysiological studies in the rat brain. *J. Pharmacol. Exp. Ther.* 347, 487–496. doi: 10.1124/jpet.113.203315

Simasko, S., and Sankaranarayanan, S. (1997). Characterization of a hyperpolarization-activated cation current in rat pituitary cells. *Am. J. Physiol.* 272 (3 Pt 1), E405–E414. doi: 10.1152/ajpendo.1997.272.3.E405

Sperling, M. R., Greenspan, A., Cramer, J. A., Kwan, P., Kälviäinen, R., Halford, J. J., et al. (2010). Carisbamate as adjunctive treatment of partial onset seizures in adults in two randomized, placebo-controlled trials. *Epilepsia* 51, 333–343. doi: 10.1111/j.1528-1167.2009.02318.x

Steriade, C., French, J., and Devinsky, O. (2020). Epilepsy: key experimental therapeutics in early clinical development. *Expert Opin. Investig. Drugs* 29, 373–383. doi: 10.1080/13543784.2020.1743678

Stojilkovic, S. S., Tabak, J., and Bertram, R. (2010). Ion channels and signaling in pituitary gland. *Endocr. Rev.* 31, 845–915. doi: 10.1210/er.2010-0005

Strzelczyk, A., and Schubert-Bast, S. (2021). Expanding the treatment landscape for Lennox-Gastaut syndrome: current and future strategies. *CNS Drugs* 35, 61–83. doi: 10.1007/s40263-020-00784-8

Taddese, A., and Bean, B. P. (2002). Subthreshold sodium current from rapidly inactivating sodium channels drives spontaneous firing of tuberomammillary neurons. *Neuron* 33, 587–600. doi: 10.1016/s0896-6273(02)00574-3

Vohora, D., Saraogi, P., Yazdani, M. A., Bhowmik, M., Khanam, R., and Pillai, K. K. (2010). Recent advances in adjunctive therapy for epilepsy: focus on sodium channel blockers as third-generation antiepileptic drugs. *Drugs Today* 46, 265–277. doi: 10.1358/dot.2010.46.4.1445795

Whalley, B. J., Strephens, G. J., and Constanti, A. (2009). Investigation of the effects of the novel anticonvulsant compound carisbamate (RWJ-333369) on rat piriform cortical neurons in vitro. *Br. J. Pharmacol.* 156, 994–1008. doi: 10.1111/j.1476-5381.2008.00110.x

Wu, P. M., Cho, H. Y., Chiang, C. W., Chuang, T. H., Wu, S. N., and Tu, Y. F. (2022a). Characterization in inhibitory effectiveness of carbamazepine in voltage-gated Na^+ and erg-mediated K^+ currents in a mouse neural crest-derived (neuro-2a) cell line. *Int. J. Mol. Sci.* 23:7892. doi: 10.3390/ijms23147892

Wu, S. N., Chern, J. H., Shen, S., Chen, H. H., Hsu, Y. T., Lee, C. C., et al. (2017). Stimulatory actions of a novel thiourea derivative on large-conductance, calcium-activated potassium channels. *J. Cell. Physiol.* 232, 3409–3421. doi: 10.1002/jcp.25788

Wu, S. N., Chiang, H. T., Shen, A. Y., and Lo, Y. K. (2003). Differential effects of quercetin, a natural polyphenolic flavonoid, on L-type calcium current in pituitary tumor (GH_3) cells and neuronal NG108-15 cells. *J. Cell. Physiol.* 195, 298–308. doi: 10.1002/jcp.10244

Wu, S. N., and Huang, C. W. (2021). Editorial to the special issue "electrophysiology". *Int. J. Mol. Sci.* 22:2956. doi: 10.3390/ijms22062956

Wu, S. N., Wu, C. L., Cho, H. Y., and Chiang, C. W. (2022b). Effective perturbations by small-molecule modulators on voltage-dependent hysteresis of transmembrane ionic currents. *Int. J. Mol. Sci.* 23:9453. doi: 10.3390/ijms23169453

Wu, S.-Z., Ye, H., Yang, Y.-G., Lu, Z.-L., Qu, Q., Qu, J. (2018). Case-control pharmacologenetic study of HCN1/HCN2 variants and genetic generalized epilespsies. *Clin. Exp. Pharmacol. Physiol.* 45, 226–233. doi: 10.1111/1440-1681.12877

Yongning, Z., Xianguang, L., Hengling, C., Su, C., Fang, L., and Chenghong, L. (2021). The hyperpolarization-activated cyclic nucleotide-gated channel currents contribute to oxaliplatin-induced hyperexcitability of DRG neurons. *Somatosens. Mot. Res.* 38, 11–19. doi: 10.1080/08990220.2020.1834376

Yu, N., Morris, C. E., Joós, B., and Longtin, A. (2012). Spontaneous excitation patterns computed for axons with injury-like impairments of sodium channels and Na/K pumps. *PLoS Comput. Biol.* 8:e1002664. doi: 10.1371/journal.pcbi.1002664